Essential role for autophagy protein ATG7 in the maintenance of intestinal stem cell integrity

Coralie Trentesaux[a], Marie Fraudeau[a], Caterina Luana Pitasi[a], Julie Lemarchand[a], Sébastien Jacques[a], Angéline Duche[a], Franck Letourneur[a], Emmanuelle Naser[a], Karine Bailly[a], Alain Schmitt[a], Christine Perret[a], and Béatrice Romagnolo[a,1]

[a]Université de Paris, Institut Cochin, INSERM, U1016, CNRS UMR8104, F-75014 Paris, France

Edited by Bert Vogelstein, Johns Hopkins Medicine Center at Johns Hopkins, Baltimore, MD, and approved March 28, 2020 (received for review October 10, 2019)

The intestinal epithelium acts as a barrier between the organism and its microenvironment, including the gut microbiota. It is the most rapidly regenerating tissue in the human body thanks to a pool of intestinal stem cells (ISCs) expressing *Lgr5*. The intestinal epithelium has to cope with continuous stress linked to its digestive and barrier functions. Epithelial repair is crucial to maintain its integrity, and Lgr5-positive intestinal stem cell (Lgr5$^+$ISC) resilience following cytotoxic stresses is central to this repair stage. We show here that autophagy, a pathway allowing the lysosomal degradation of intracellular components, plays a crucial role in the maintenance and genetic integrity of Lgr5$^+$ISC under physiological and stress conditions. Using conditional mice models lacking the autophagy gene *Atg7* specifically in all intestinal epithelial cells or in Lgr5$^+$ISC, we show that loss of Atg7 induces the p53-mediated apoptosis of Lgr5$^+$ISC. Mechanistically, this is due to increasing oxidative stress, alterations to interactions with the microbiota, and defective DNA repair. Following irradiation, we show that Lgr5$^+$ISC repair DNA damage more efficiently than their progenitors and that this protection is Atg7 dependent. Accordingly, we found that the stimulation of autophagy on fasting protects Lgr5$^+$ISC against DNA damage and cell death mediated by oxaliplatin and doxorubicin treatments. Finally, *p53* deletion prevents the death of *Atg7*-deficient Lgr5$^+$ISC but promotes genetic instability and tumor formation. Altogether, our findings provide insights into the mechanisms underlying maintenance and integrity of ISC and highlight the key functions of Atg7 and p53.

Atg7 | autophagy | intestinal stem cells | DNA repair

The intestinal epithelium is a highly organized hierarchy originating from a pool of proliferative stem cells characterized by their expression of the leucine-rich repeat-containing G protein-coupled receptor 5 (LGR5). These Lgr5-positive intestinal stem cells (Lgr5$^+$ISC) reside at the bottom of the intestinal crypts of Lieberkühn and are in direct contact with Paneth cells, which contribute to the niche by secreting Wnt ligands (1). Lgr5$^+$ISC give rise to transit-amplifying (TA) progenitors that move toward the crypt–villus junction and differentiate into the two differentiated lineages of the epithelium: absorptive enterocytes and secretory lineage cells, including Paneth cells, goblet cells, and enteroendocrine cells (2). Lgr5$^+$ISC are, therefore, essential for the regeneration of epithelial cells, which have a turnover of 3 to 5 d at homeostasis. Lgr5$^+$ISC are crucial for epithelial repair following cytotoxic stress (3) and are thought to be one of the cell types from which colorectal cancers originate (4). The lifelong maintenance of intestinal homeostasis requires preservation of the functional and genomic integrity of Lgr5$^+$ISC in the face of various infectious, physical, or chemical stresses. These cells may, thus, be equipped with unique mechanisms to ensure their protection and survival. The signaling pathways responsible for the proliferation and self-renewal of Lgr5$^+$ISC are well known, but much less is known about the mechanisms controlling their integrity and resilience in conditions of cytotoxic stress.

Autophagy is an evolutionarily conserved pathway through which cellular materials are targeted to the lysosomes for degradation. At basal levels, this cellular process eliminates damaged components that threaten cell integrity, but it also acts as a major adaptive stress response, with functions ranging from providing starving cells with metabolic sustenance to warding off microbial attacks (5). Autophagy also plays an important role in tumor development in several tissues, including the intestine. We have shown that autophagic activity is enhanced during colorectal cancer development (6). Using mice lacking the essential autophagy gene *Atg7* specifically in intestinal epithelial cells, we showed that Atg7 was required for both tumor initiation and intestinal tumor cell metabolism. We extended these results by showing that the loss of Atg7 affects the mucosal microenvironment by shaping an antitumoral immune response linked to a change in the composition of the microbiota. Recent work has suggested that autophagic mechanisms are highly active in intestinal stem cells (ISC) and seem critical for their maintenance. Deletion of the Atg5 gene in intestinal epithelial cells results in accumulation of mitochondria and reactive oxygen species (ROS) in Lgr5$^+$ISC and impaired their capacity to induce intestinal regeneration following irradiation (7). In this study, we show that Atg7, another key autophagy gene, is also required for Lgr5$^+$ISC fitness. We show that homeostatic Lgr5$^+$ISC are particularly sensitive to the deletion of *Atg7*. Unlike differentiated

Significance

Studies on intestinal stem cells (ISC) have increased our understanding of stem cell dynamics, tissue plasticity, and tumor-initiating cells. However, the molecular mechanisms involved in the maintenance and integrity of this stem cell pool remain unclear. Using conditional mice models lacking the autophagy gene *Atg7* in intestinal epithelial cells and specifically, in ISC, we show that Atg7 contributes to the unique characteristic of ISC and demonstrate its importance to promote efficient DNA damage repair and survival on homeostasis and following cytotoxic stresses. These findings highlight the translational potential of autophagy activation to induce epithelial regeneration and to protect host toxicity in patients undergoing high doses of chemotherapy or radiotherapy.

Author contributions: C.T. and B.R. designed research; C.T., M.F., C.L.P., and J.L. performed research; S.J., A.D., F.L., E.N., K.B., and A.S. contributed new reagents/analytic tools; C.T., M.F., C.L.P., C.P., and B.R. analyzed data; and C.T. and B.R. wrote the paper.

The authors declare no competing interest.

This article is a PNAS Direct Submission.

Data deposition: Microarray data generated in this study are available in the Gene Expression Omnibus (accession no. GSE136952).

[1]To whom correspondence may be addressed. Email: beatrice.romagnolo@inserm.fr.

This article contains supporting information online at https://www.pnas.org/lookup/suppl/doi:10.1073/pnas.1917174117/-/DCSupplemental.

First published May 5, 2020.

cells and TA progenitors, Atg7-deficient Lgr5^{+}ISC have defective antioxidant and DNA repair responses, resulting in the accumulation of cytotoxic damage and the induction of p53-mediated apoptosis. The blockade of p53 prevents the death of Atg7-deficient Lgr5^{+}ISC and promotes genetic instability and tumor initiation. These results indicate that Atg7 and p53 act together to protect the integrity of Lgr5^{+}ISC. We also show that *Atg7* deletion sensitizes Lgr5^{+}ISC to irradiation and chemotherapy. Conversely, we found that stimulating autophagy in intestinal crypts on fasting protected Lgr5^{+}ISC against the cytotoxic damage induced by chemotherapy. Finally, we show that Paneth cell defects associated with the loss of *Atg7* do not affect the niche function of these cells but contribute to the apoptosis of Lgr5^{+}ISC through an antimicrobial defense defect, revealing close links between the microbiota, Atg7, and Lgr5^{+}ISC integrity.

Results

Atg7 Loss Induces the Apoptosis of Lgr5^{+}ISC. We investigated the impact of autophagy on intestinal epithelial cell homeostasis by studying VillinCreER^{T2}Atg7$^{fl/fl}$ mice in which Atg7 is conditionally knocked out in intestinal epithelial cells on tamoxifen injection (hereafter referred to as Atg7$^{-/-}$ mice). We confirmed the loss of ATG7 and the inhibition of autophagy by evaluating LC3-II (microtubule-associated protein Light Chain 3) expression and accumulation of the typical autophagy target proteins p62 and ubiquitin as aggregates in both the differentiated villi and proliferative crypts (*SI Appendix*, Fig. S1 *A* and *B*). Our results indicated that autophagy was effectively inhibited throughout the intestinal epithelium. Despite the rapid turnover of the epithelium, this phenotype was maintained over time, confirming the loss of *Atg7* from the ISC compartment.

Atg7 knockout in all intestinal epithelial cells led to the appearance of TUNEL (terminal deoxynucleotidyl transferase dUTP nick end labeling)-positive cells, particularly at the base of the Atg7$^{-/-}$ crypts, together with an accumulation of nuclear p53 and cleaved caspase-3 (Fig. 1 *A* and *B*). TUNEL-positive cells colocalized with the Lgr5^{+}ISC marker Olfm4, and their distribution was mutually exclusive with that of the Paneth cell product lysozyme (Fig. 1*C*), indicating that Lgr5^{+}ISC and not Paneth cells underwent apoptosis following *Atg7* knockout.

Lgr5^{+}ISC death was sustained over time but was not detrimental to epithelial regeneration as a pool of Lgr5^{+}ISC was maintained and lifespan was similar in Atg7$^{-/-}$ mice and controls. An increase in crypt height associated with a higher level of BrdU (Bromodeoxyuridine) incorporation was observed in ATG7-deficient crypts together with an expansion of the expression of Lgr5^{+}ISC markers (*SI Appendix*, Fig. S1 *C–E*),

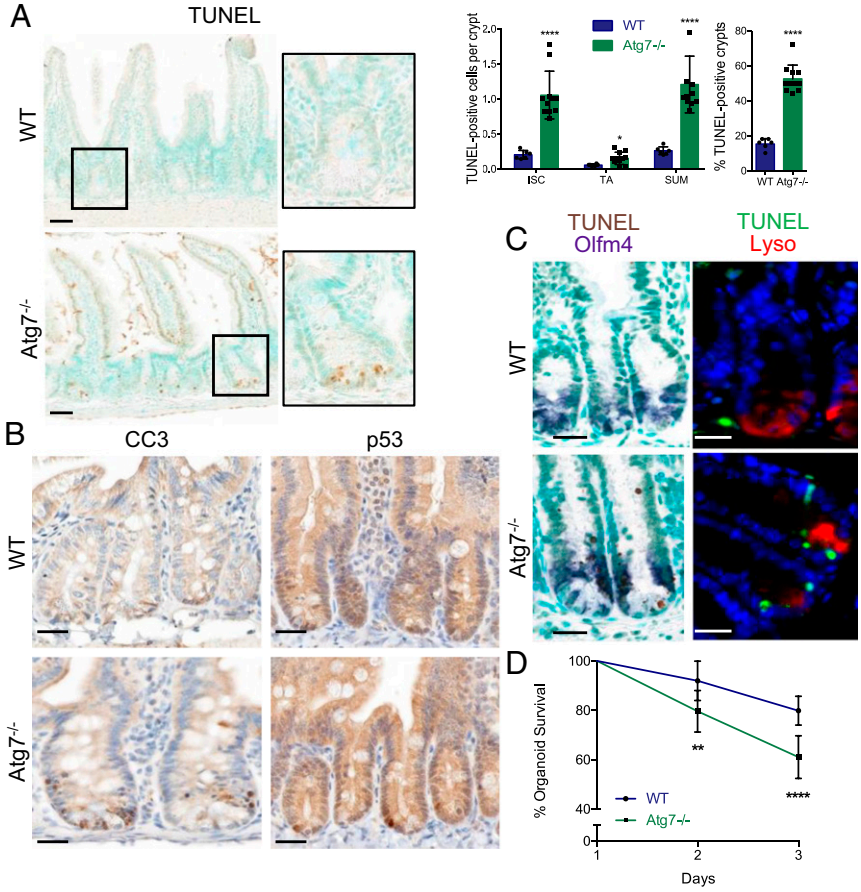

Fig. 1. Atg7 deletion throughout the intestinal epithelium leads to Lgr5^{+}ISC apoptosis. (*A*) Representative TUNEL staining on WT (wild type) and Atg7$^{-/-}$ tissue sections. Methyl green was used as a nuclear counterstain. Quantification of the percentage of TUNEL-positive crypts and the mean number of TUNEL-positive cells per crypt over 50 consecutive whole crypts in 6 WT and 11 Atg7$^{-/-}$ mice. The data shown are means ± SD. (Scale bars: 50 μm.) (*B*) Representative cleaved caspase-3 and p53 staining on tissue sections from WT and Atg7$^{-/-}$ intestines. (Scale bars: 25 μm.) (*C*) Representative TUNEL staining combined with in situ hybridization for Olfm4. Representative TUNEL staining combined with lysozyme staining. (Scale bars: 25 μm.) (*D*) Percentage survival from day 1 of organoids from the crypts of WT and Atg7$^{-/-}$ mice ($n = 9$ mice for WT and $n = 7$ mice for Atg7$^{-/-}$). The data shown are means ± SD. Significant differences are shown with asterisks. *$P < 0.05$; **$P < 0.01$; ****$P < 0.0001$.

suggesting that the surviving ISC, early progenitors, or another ISC pool might have higher levels of proliferation in these mice, potentially accounting for the replenishment of Lgr5^{+}ISC. We quantified mRNA (messenger RNA) for the proposed "+4" reserve ISC markers and found no significant difference in their expression between Atg7$^{-/-}$ mice and controls, although the involvement of such a population cannot be ruled out (*SI Appendix*, Fig. S1*F*).

We then assessed the capacity of isolated crypts from tamoxifen-treated WT and Atg7$^{-/-}$ mice to develop into intestinal organoids ex vivo. Survival was significantly lower for Atg7-deficient organoids than for WT organoids, revealing a stem cell defect (Fig. 1*D*). We also found TUNEL-positive cells in the crypts of Atg7$^{-/-}$ organoids, consistent with the in vivo phenotype (*SI Appendix*, Fig. S1*G*).

Atg7-Deficient Lgr5^{+}ISC Apoptosis Is Dependent on p53. We investigated the molecular events resulting in the death of Lgr5^{+}ISC following Atg7 deletion. We and others have described defects in the secretory lineage, affecting Paneth cells in particular, in autophagy-deficient mice (6, 8, 9). Paneth cells are found in close proximity to Lgr5^{+}ISC and secrete both protective antimicrobial peptides and growth factors essential to the stem cell niche. Consistent with published findings, the Paneth cells of Atg7$^{-/-}$ mice produced only small amounts of antimicrobial peptides, and their lysozyme distribution was abnormal (*SI Appendix*, Fig. S2 *A* and *B*). By contrast, the expression of Paneth cell niche factors, including Wnt and Notch ligands, was not affected by *Atg7* knockout (*SI Appendix*, Fig. S2*C*). Moreover, the addition of exogenous Wnt ligand to the culture medium did not rescue the survival of *Atg7*-deficient organoids (*SI Appendix*, Fig. S2*D*). The death of autophagy-deficient Lgr5^{+}ISC is probably, therefore, independent of Paneth cell niche function.

By contrast, the addition of the p53 inhibitor pifithrin to the organoid culture medium rescued the survival defect of Atg7-deficient organoids (Fig. 2*A*). To confirm the role of p53 in Atg7-deficient Lgr5^{+}ISC death in vivo, we crossed Villin-CreER^{T2}Atg7$^{fl/fl}$ mice with p53$^{fl/fl}$ mice, resulting in the simultaneous loss of both ATG7 and p53 proteins in the resulting progeny on tamoxifen injection (hereafter referred to as Atg7$^{-/-}$p53$^{-/-}$ mice) as confirmed by western blotting and immunohistochemistry (Fig. 2 *B* and *C*). Atg7$^{-/-}$p53$^{-/-}$ crypts contained significantly fewer TUNEL-positive cells than Atg7$^{-/-}$ crypts (Fig. 2*C*), confirming the dependence of the apoptosis of Atg7-deficient Lgr5^{+}ISC on p53. Consistent with these findings, survival was higher for organoids from Atg7$^{-/-}$p53$^{-/-}$ crypts than for organoids from Atg7$^{-/-}$ crypts (Fig. 2*D*).

Atg7 Promotes Efficient DNA Damage Repair and Survival in Lgr5^{+}ISC. We investigated the role of Atg7 in Lgr5^{+}ISC by crossing Lgr5-EGFP-CreER^{T2} knock-in mice (Lgr5WT) with Atg7$^{fl/fl}$ mice. In the resulting Lgr5-EGFP (enhanced green fluorescent protein)-CreER^{T2}Atg7$^{fl/fl}$ mice, *Atg7* was conditionally knocked out in Lgr5^{+}ISC following the injection of tamoxifen. It was thus also knocked out in the daughter intestinal epithelial cells over time, resulting in Lgr5Atg7$^{-/-}$ mice. We confirmed the effective inhibition of autophagy in these mice by demonstrating p62 accumulation in the EGFP-positive crypts of these mice after tamoxifen treatment (*SI Appendix*, Fig. S3*A*). Using this model, we were able to sort Lgr5^{+}ISC and their early TA progenitors from both Lgr5WT and Lgr5Atg7$^{-/-}$ crypts on the basis of EGFP expression (EGFP^{High} for Lgr5^{+}ISC and EGFP^{Low} for TA cells) (*SI Appendix*, Fig. S3*B*). We first confirmed by qRT-PCR the enhanced expression of ISC markers in EGFP^{High} populations and the effective loss of *Atg7* expression in this population following tamoxifen treatment (*SI Appendix*, Fig. S3*B*). Microarray expression profiling of Lgr5^{+}ISC from Lgr5Atg7$^{-/-}$ and Lgr5WT crypts identified 2,334 genes displaying significantly altered expression in the ISC population, whereas 825 genes were significantly deregulated in TA progenitors. Only 46 of these genes were deregulated in both the ISC and TA signatures following the loss of *Atg7* (*SI Appendix*, Fig. S3*C*), revealing markedly different responses in these two populations. We, therefore, focused our analysis on signatures specific to Lgr5^{+}ISC that might explain their particular sensitivity to the loss of *Atg7*.

The top-ranking canonical pathways identified by Ingenuity Pathway Analysis revealed an effect of the loss of *Atg7* on the DNA damage response in Lgr5^{+}ISC, the affected pathways including ATM (ataxia-telangiectasia mutated) signaling, BRCA1 in DNA damage response, and CHK proteins in cell cycle checkpoint control (*SI Appendix*, Fig. S3*D*, yellow arrowheads). Likewise, Gene Set Enrichment Analysis (GSEA) revealed an enrichment in the expression of DNA repair and G2/M checkpoint genes in WT Lgr5^{+}ISC relative to their Atg7$^{-/-}$ counterparts (Fig. 3*A*). We, therefore, investigated DNA damage in situ in WT and Atg7$^{-/-}$ mice. We detected frequent zones of γH2AX (gamma-histone H2AX) foci in the Atg7$^{-/-}$ epithelium, indicating the occurrence of unrepaired double-stranded DNA breaks. Moreover, these foci were located specifically in the ISC compartment of the crypt (Fig. 3*B*). High levels of DNA damage in autophagy-deficient Lgr5^{+}ISC may result from inefficient DNA repair, contributing to the impaired survival of these cells. We assessed the effect of Atg7 deletion on the DNA damage response pathways guaranteeing genomic integrity more directly by evaluating the effect of γ-irradiation (10 Gy) on WT and Atg7$^{-/-}$ mice. Six hours after irradiation, control mice presented numerous γH2AX foci in their crypt compartment but relatively fewer in the Lgr5^{+}ISC (Fig. 3*C*). The loss of Atg7 increased DNA damage specifically in Lgr5^{+}ISC, which presented many γH2AX foci, and induced their apoptosis (Fig. 3*D*). These data indicate that Lgr5^{+}ISC repair DNA damage more efficiently than their progenitors and that this protection is Atg7 dependent.

Fasting Protects against DNA Damage by Activating Autophagy. As inhibiting Atg7 sensitized Lgr5^{+}ISC to DNA damage, we investigated whether stimulating autophagy could improve Lgr5^{+}ISC function and survival in response to genotoxic stress. We used a 24-h fasting protocol, which is known to induce autophagy in various tissues (10, 11). We first validated the effects of fasting on autophagy by looking at the conversion of LC3-I to LC3-II in organoids derived from ad libitum-fed and fasted WT mice. LC3-II accumulated more strongly in organoids derived from fasted mice and treated with chloroquine for lysosomal inhibition, confirming that fasting increases autophagy flux in intestinal epithelial cells (Fig. 4*A*). Accordingly, LC3 foci, which are in situ indicators of autophagosomes, increased in number by a factor of six in the crypts of control mice subjected to a 24-h fast (Fig. 4*B*), whereas no such increase was observed in fasted mutant mice.

The 24-h fast was then followed by two types of chemotherapy treatment known to induce double-stranded DNA breaks (oxaliplatin and doxorubicin), and DNA damage was assessed by γH2AX staining. Within 6 h of either of these two treatments, significantly more ISC presented double-stranded breaks in *Atg7*-deficient crypts than in WT crypts (Fig. 4*C* and *SI Appendix*, Fig. S4*A*). This finding is consistent with our previous findings for irradiation. WT mice fasted for 24 h before treatment had significantly fewer γH2AX-positive Lgr5^{+}ISC within 6 h of oxaliplatin or doxorubicin treatment (Fig. 4*C* and *SI Appendix*, Fig. S4*A*). This was not the case for the Lgr5^{+}ISC of Atg7-depleted crypts, which had similarly high levels of γH2AX staining following both these treatments, regardless of prior feeding regimen. Accordingly, there were significantly more TUNEL-positive cells in the Lgr5^{+}ISC compartment of Atg7-deficient crypts than in WT crypts after treatment with either oxaliplatin or doxorubicin (Fig. 4*D* and *SI Appendix*, Fig. S4*B*). The

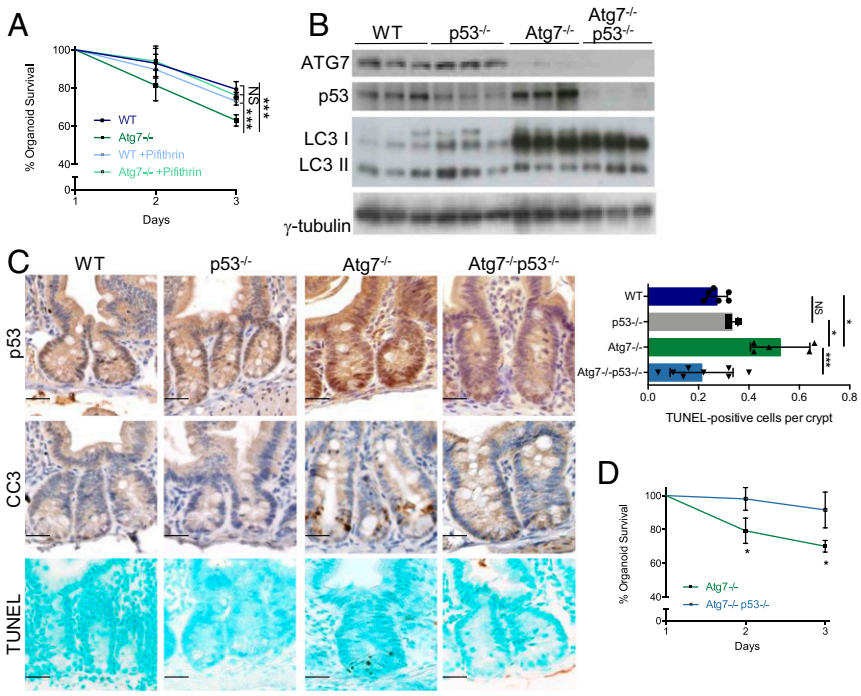

Fig. 2. Atg7-deficient Lgr5$^+$ISC apoptosis is dependent on p53. (*A*) Percentage survival from day 1 of organoids from the crypts of WT and Atg7$^{-/-}$ mice in the presence or absence of pifithrin in the culture medium (n = 3 mice of each genotype). Significant differences are shown for day 3. (*B*) Western blotting for ATG7, p53, and LC3 on whole-intestinal tissue lysates from WT, p53$^{-/-}$, Atg7$^{-/-}$, and Atg7$^{-/-}$p53$^{-/-}$ mice. γ-Tubulin was used as a loading control. Results are shown for three individual mice of each genotype. (*C*) Representative p53, CC3, and TUNEL staining in the crypts of WT, p53$^{-/-}$, Atg7$^{-/-}$, and Atg7$^{-/-}$p53$^{-/-}$ mice. Quantification of the mean number of TUNEL-positive cells per crypt over 50 consecutive whole crypts in seven WT, three p53, five Atg7$^{-/-}$, and eight Atg7$^{-/-}$p53$^{-/-}$ mice. The data shown are means ± SD. (Scale bars: 25 μm.) (*D*) Percentage survival from day 1 of organoids from the crypts of Atg7$^{-/-}$ and Atg7$^{-/-}$p53$^{-/-}$ mice (n = 3 mice of each genotype). Significant differences are shown with asterisks. NS, not statistically significant. *P < 0.05; ***P < 0.005.

Lgr5$^+$ISC survival was doubled by fasting in WT mice treated with oxaliplatin and tripled in WT mice treated with doxorubicin. By contrast, fasting had no significant effect on the survival of *Atg7*-deficient Lgr5$^+$ISC (Fig. 4*D* and *SI Appendix*, Fig. S4*B*). Thus, fasting seems to protect Lgr5$^+$ISC from chemotherapy-induced DNA damage and cell death in an *Atg7*-dependent manner. We studied the effect of these treatments on ISC function by culturing crypts from fasted or fed mice treated with oxaliplatin or doxorubicin for 6 h. Survival was extremely low for organoids grown from the crypts of mice treated with either oxaliplatin or doxorubicin. Fasting significantly improved the survival of WT but not Atg7$^{-/-}$ organoids (*SI Appendix*, Fig. S4*C*). These results provide further evidence for an *Atg7*-dependent protective effect of fasting on Lgr5$^+$ISC function. Overall, our data suggest that the *Atg7*-dependent up-regulation of autophagy in intestinal crypts on fasting protects Lgr5$^+$ISC from DNA damage and cell death on exposure to genotoxic chemotherapy agents.

The Accumulation of ROS Renders *Atg7*-Deficient Lgr5$^+$ISC More Sensitive to Apoptosis. GSEA also revealed an enrichment in signatures linked to the detoxification of ROS, including NRF2 target genes, in Lgr5$^+$ISC from Lgr5WT mice relative to their counterparts from Lgr5Atg7$^{-/-}$ mice (Fig. 5*A*). This result is surprising as autophagy inhibition has been shown to drive NRF2 stabilization and transcriptional activity in a p62-dependent manner (12). Consistent with this mechanism and with p62 accumulation, we observed an increase in NRF2 protein levels (Fig. 5*B*) and an up-regulation of the expression of the antioxidant target genes of this protein on qRT-PCR analyses (Fig. 5*C*) of whole intestinal tissues from Atg7$^{-/-}$ mice. However, qRT-PCR on sorted Atg7$^{-/-}$ Lgr5$^+$ISC confirmed the predicted down-regulation of NRF2 target genes relative to the WT counterparts of these cells (Fig. 5*D*). This down-regulation of the NRF2 response may also contribute to the high sensitivity of Lgr5$^+$ISC to Atg7 deletion.

In light of the divergent responses between Lgr5$^+$ISC and the other cells of the tissue, we assessed ROS levels directly in Lgr5$^+$ISC with the cytoplasmic ROS-responsive fluorescent probe CellROX. Flow cytometry revealed a significantly higher mean fluorescence intensity for CellROX in Atg7$^{-/-}$ Lgr5$^+$ISC than in their WT counterparts (Fig. 5*E*). Similarly, CellROX fluorescence was much stronger at the base of Atg7$^{-/-}$ organoid crypts than at the base of WT organoid crypts (Fig. 5*F*), demonstrating the presence of higher levels of ROS in the Lgr5$^+$ISC compartment of Atg7-deficient crypts. We investigated the contribution of the antioxidant response and ROS accumulation to autophagy-deficient ISC death by treating Atg7$^{-/-}$ organoids with *N*-acetyl cysteine (NAC), a precursor of glutathione and a direct ROS scavenger, or sulforaphane, an activator of NRF2 signaling. Both NAC and sulforaphane treatments decreased the intensity of CellROX fluorescence in organoid crypts (Fig. 5*F*) and partially rescued Atg7-deficient organoid survival (Fig. 5*G*), suggesting that ROS accumulation contributes to the death of Atg7-deficient Lgr5$^+$ISC. We tested this hypothesis in vivo by adding NAC to the drinking water of Atg7$^{-/-}$ and WT mice. As expected, NAC treatment significantly decreased the number of TUNEL-positive cells in Atg7$^{-/-}$ crypts (Fig. 5*H*). The inhibition of Atg7, therefore, led to an unexpected down-regulation of the antioxidant response in Lgr5$^+$ISC, rendering them more prone to ROS accumulation and apoptosis.

We investigated the potential sources of ROS in the Atg7-deficient epithelium. Autophagy is linked to the antioxidant response but can also directly regulate ROS production through the selective degradation of mitochondria, a major cellular source of ROS, in a process known as mitophagy. Transmission electron microscopy revealed the presence of abnormally large,

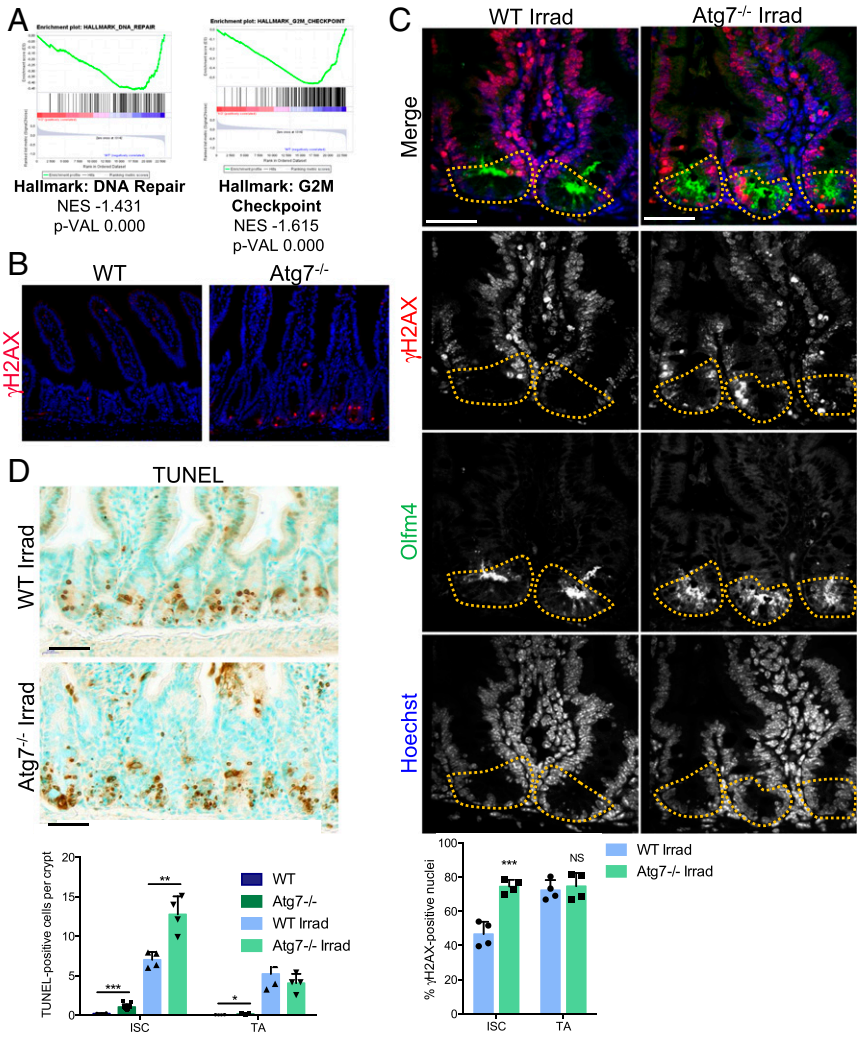

Fig. 3. Loss of Atg7 disrupts DNA damage repair in Lgr5^{+}ISC. (*A*) Enrichment plots generated by GSEA for hallmark DNA repair and G2/M checkpoint gene sets based on transcriptomic data for GFP^{High} Lgr5^{+}ISC from the crypts of Lgr5Atg7$^{-/-}$ vs. Lgr5WT mice. NES, normalized enrichment score; p-VAL, *P* value. (*B*) γH2AX staining showing a lack of epithelial staining in WT crypts and a representative positive zone in the Atg7$^{-/-}$ epithelium. (Scale bars: 50 μm.) (*C*) Representative *z* projection (from 20 stacks spanning over 6 μm to include whole nuclei) of combined γH2AX and Olfm4 staining in the crypts of WT and Atg7$^{-/-}$ mice 6 h after 10-Gγ whole-body irradiation. Yellow dashed lines indicate the Lgr5^{+}ISC compartment. The percentage of γH2AX-positive cells was determined on at least 10 randomly selected whole crypts per mouse ($n = 4$ mice of each genotype). Cells with more than four γH2AX foci in their nuclei were considered γH2AX positive. Olfm4^{+} cells were considered to be ISC, and the Olfm4^{-} cells above them and below the crypt–villus junction were considered to be TA cells. The data shown are means ± SD. (Scale bars: 50 μm.) (*D*) Representative TUNEL staining on tissue sections from WT and Atg7$^{-/-}$ mice 6 h after 10-Gγ whole-body irradiation. Determination of the mean number of TUNEL-positive cells per crypt over 50 consecutive whole crypts in 6 control WT mice, 11 control Atg7$^{-/-}$ mice, and 4 irradiated mice of each genotype. The data shown are means ± SD. Significant differences are shown with asterisks. NS, not statistically significant. (Scale bars: 50 μm.) *$P < 0.05$; **$P < 0.01$; ***$P < 0.005$.

swollen mitochondria throughout the epithelium of Atg7$^{-/-}$ mice, including the Lgr5^{+}ISC (*SI Appendix*, Fig. S5*A*). Surprisingly, mitochondrial numbers were unaffected by the inhibition of autophagy whether determined for the entire intestinal tissue by qRT-PCR on mitochondrial DNA (*SI Appendix*, Fig. S5*B*) or in sorted Lgr5^{+}ISC with the fluorescent probe MitoTracker (*SI Appendix*, Fig. S5*C*). The high proliferation rates of Lgr5^{+}ISC may account for the lack of accumulation of mitochondria despite the inhibition of their degradation pathway. Nevertheless, in addition to the unusual mitochondrial morphology, we also observed a significant increase in mitochondrial ROS production in Atg7-deficient Lgr5^{+}ISC on flow cytometry with the fluorescent probe MitoSOX (Fig. 5*E*). Defective mitochondria may, therefore, act as a cell-intrinsic source of ROS in the autophagy-deficient epithelium, acting together with down-regulation of the antioxidant response to impair the survival of Atg7-deficient Lgr5^{+}ISC.

The Gut Microbiota Contributes to the Death of *Atg7*-Deficient Lgr5^{+}ISC. We previously showed that faulty antimicrobial defenses following the loss of Atg7 throughout the intestinal epithelium, including defects in antimicrobial peptide production by Paneth cells (*SI Appendix*, Fig. S2 *A* and *B*), altered contact with the microbiota and disrupted the resident gut bacterial communities (6). We investigated the potential effect of the altered microbiota on Lgr5^{+}ISC survival by orally administering broad-spectrum antibiotics to WT and Atg7$^{-/-}$ mice. This antibiotic treatment significantly decreased the number of TUNEL-positive cells in Atg7$^{-/-}$ crypts (Fig. 6*A*), suggesting an involvement of the microbiota in the disruption of ISC homeostasis. Consistently, antibiotic-treated Atg7$^{-/-}$ mice had few if any γH2AX-positive zones and

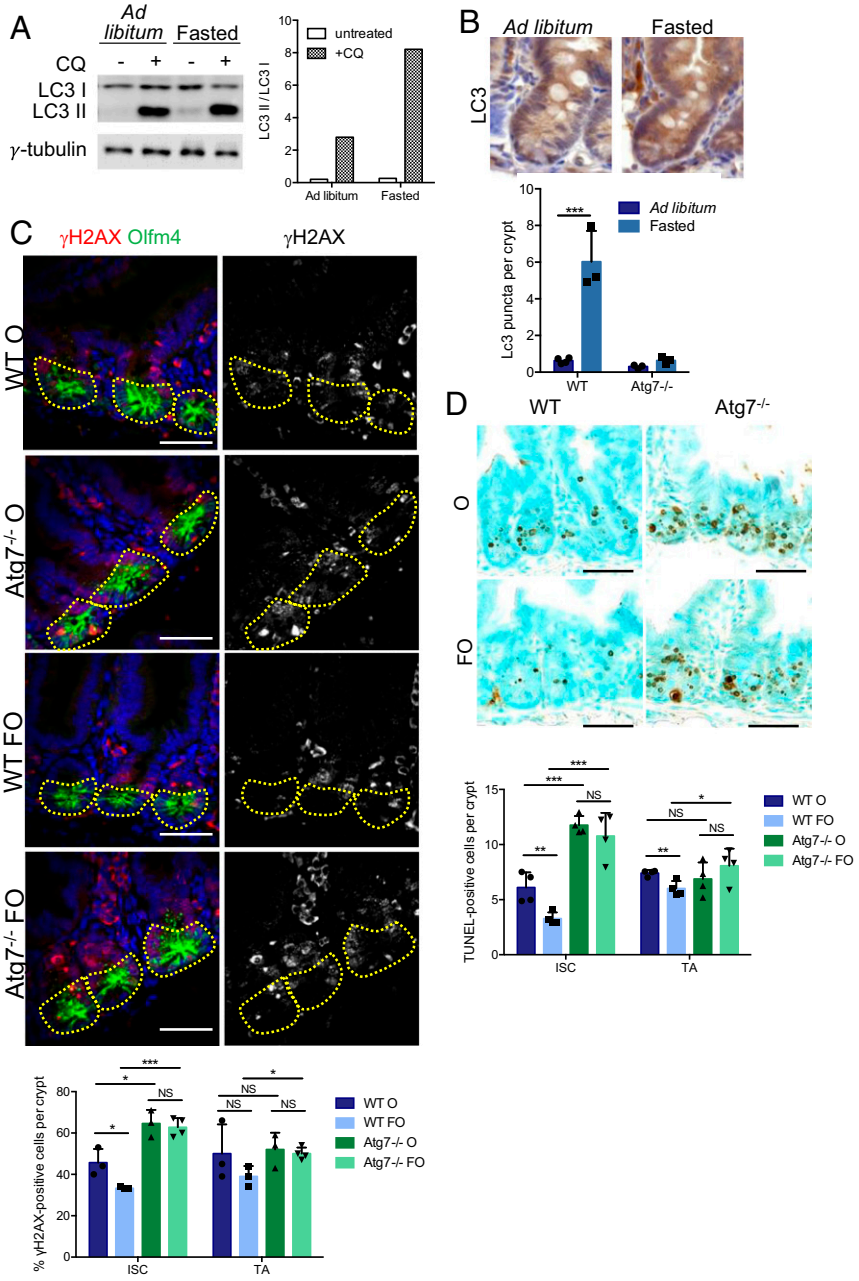

Fig. 4. Fasting protects ISC from chemotherapy-induced DNA damage and apoptosis in an Atg7-dependent manner. (*A*) Western blotting for LC3 in organoids derived from WT mice that were either fed ad libitum or fasted for 24 h. Chloroquine (CQ) was used to block autophagic flux. γ-Tubulin was used as a loading control. (*B*) Representative LC3 staining in WT crypts from mice either fed ad libitum or fasted for 24 h. Quantification of LC3 puncta per crypt in WT and Atg7$^{-/-}$ mice either fed ad libitum or fasted for 24 h. (*C*) Representative *z* projection (from 20 stacks spanning 6 μm to include whole nuclei) of combined γH2AX and Olfm4 staining and γH2AX staining alone (*Right*) in the crypts of WT and Atg7$^{-/-}$ mice 6 h after oxaliplatin treatment alone (O) or preceded by a 24-h fast (FO). The percentage of γH2AX-positive cells was determined on at least 10 randomly selected whole crypts per mouse (n = 4 mice of each genotype). Cells with more than four γH2AX foci in their nuclei were considered γH2AX positive. Olfm4^{+} cells (circled area) were considered to be ISC, and the Olfm4^{-} cells above them and below the crypt–villus junction were considered to be TA cells. The data shown are means ± SD. (Scale bars: 50 μm.) (*D*) Representative TUNEL staining of tissue sections from WT and Atg7$^{-/-}$ mice after 6 h of oxaliplatin treatment alone (O) or preceded by a 24-h fast (FO). Determination of the mean number of TUNEL-positive cells per crypt over 50 consecutive whole crypts in four mice per condition. The data shown are means ± SD. Significant differences are shown with asterisks. NS, not statistically significant. (Scale bars: 50 μm.) *P < 0.05; **P < 0.01; ***P < 0.005.

displayed no global induction of antioxidant response genes (*SI Appendix*, Fig. S6), consistent with a lower level of cytotoxic stress accumulation in the autophagy-deficient epithelium in the absence of the microbiota.

We used organoid culture to distinguish between the epithelium-intrinsic and microenvironment-dependent effects of Atg7 deletion in ISC. Organoids derived from the crypts of tamoxifen-treated Atg7$^{-/-}$ mice conserved the Lgr5^{+}ISC defects (Fig. 1*D*), but neither the knockout of *Atg7* ex vivo by the addition of 4-hydroxy-tamoxifen (4OHT) to crypt culture medium nor treatment with chloroquine affected organoid survival (Fig. 6 *B* and *C*), despite the efficient inhibition of autophagic

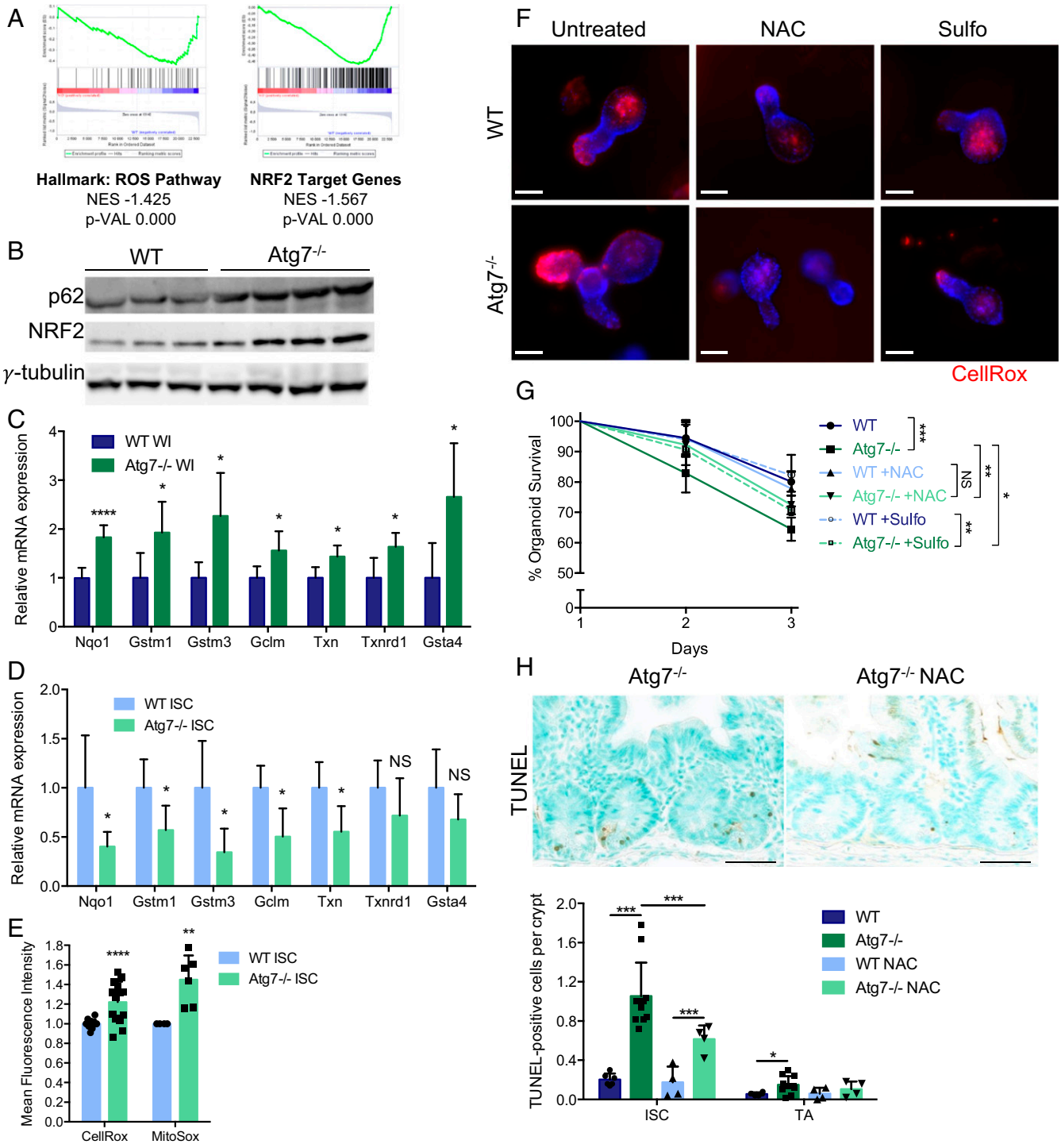

Fig. 5. Defective antioxidant responses and ROS accumulation contribute to the death of Atg7-deficient Lgr5^{+}ISC. (*A*) Enrichment plots generated by GSEA for the hallmark ROS pathway and NRF2 target gene sets based on transcriptomic data from sorted Lgr5^{+}ISC from Lgr5Atg7$^{-/-}$ and Lgr5WT mice. NES, normalized enrichment score; p-VAL, *P* value. (*B*) Western blotting for p62 and NRF2 on whole-intestinal (WI) tissue lysates from WT and Atg7$^{-/-}$ mice. γ-Tubulin was used as a loading control. Three WT and four Atg7$^{-/-}$ mice are shown. (*C*) Relative mRNA levels for NRF2 target genes encoding antioxidant response proteins as assessed by qRT-PCR analysis of whole-intestinal tissue lysates from four WT and five Atg7$^{-/-}$ mice. The data shown are means ± SD. (*D*) Relative mRNA levels for NRF2 target genes encoding antioxidant response proteins as assessed by qRT-PCR analysis of sorted Lgr5^{+}ISC from Lgr5WT and Lgr5Atg7$^{-/-}$ mice. The data shown are means ± SD ($n = 4$ to 6 mice per condition). (*E*) Mean CellROX or MitoSOX fluorescence intensity of sorted Lgr5^{+}ISC from Lgr5WT and Lgr5Atg7$^{-/-}$ mice. The data shown are means ± SD ($n = 13$ Lgr5WT and $n = 14$ Lgr5Atg7$^{-/-}$ mice for CellROX analysis, $n = 4$ Lgr5WT and $n = 6$ Lgr5Atg7$^{-/-}$ mice for MitoSOX analysis). (*F*) Representative CellROX staining on live organoids from the crypts of WT and Atg7$^{-/-}$ mice after 3 d in culture in the presence or absence of NAC or sulforaphane (Sulfo) in the culture medium. Hoechst stain was used as a nuclear counterstain. (Scale bars: 50 μm.) (*G*) Percentage survival from day 1 of organoids from the crypts of WT and Atg7$^{-/-}$ mice in the presence or absence of NAC or Sulfo in the culture medium ($n = 5$ mice for each genotype). Significant differences are shown in the legend for day 3. (*H*) Representative TUNEL staining on tissue sections from Atg7$^{-/-}$ mice treated with water or NAC. Quantification of the percentage of TUNEL-positive crypts and the mean number of TUNEL-positive cells per crypt over 50 consecutive whole crypts in 6 control WT mice, 11 control Atg7$^{-/-}$ mice, and 4 NAC-treated mice of each genotype. The data shown are means ± SD. Significant differences are shown with asterisks. NS, not statistically significant. (Scale bars: 50 μm.) *$P < 0.05$; **$P < 0.01$; ***$P < 0.005$; ****$P < 0.001$.

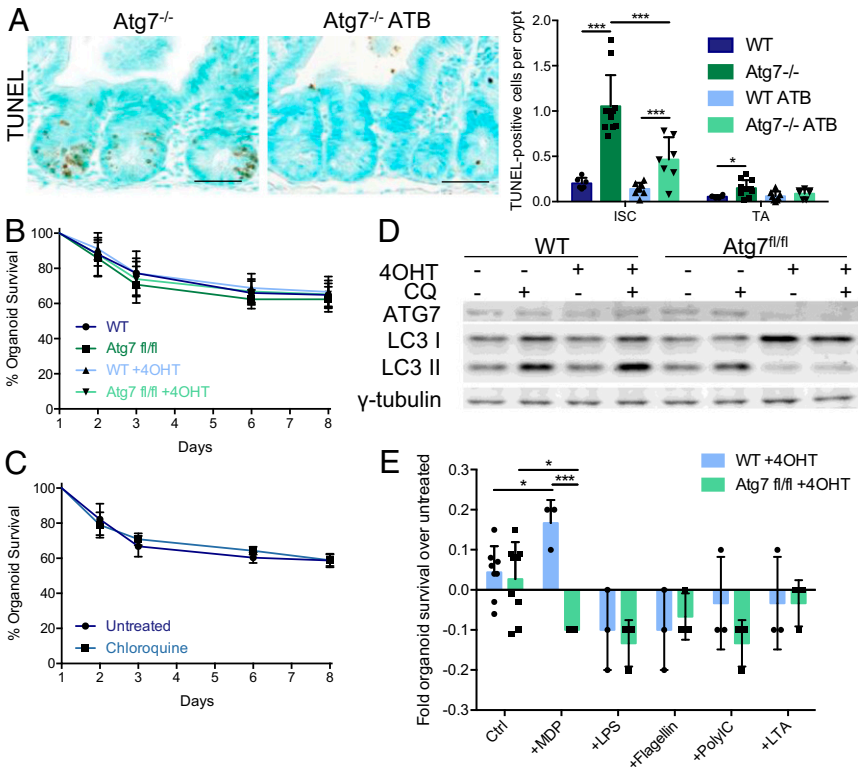

Fig. 6. Interactions with the microbiota contribute to the apoptosis of Atg7-deficient Lgr5^{+}ISC. (*A*) Representative TUNEL staining on tissue sections of Atg7$^{-/-}$ mice treated with water or broad-spectrum antibiotics (ATB). Quantification of the mean number of TUNEL-positive cells per crypt over 50 consecutive whole crypts in 6 control WT mice, 11 control Atg7$^{-/-}$ mice, 8 WT, and 7 Atg7$^{-/-}$ ATB-treated mice. The data shown are means ± SD. (Scale bars: 50 μm.) (*B*) Percentage survival from day 1 of WT or Atg7$^{fl/fl}$ organoids in the presence or absence of 4OHT in the culture medium ($n = 6$ mice per condition). (*C*) Percentage survival from day 1 of WT organoids in the presence or absence of chloroquine (CQ) in the culture medium ($n = 6$ mice per condition). (*D*) Western blotting for ATG7 and LC3 on protein extracts from day 4 WT or Atg7$^{fl/fl}$ organoids in the presence or absence of 4OHT and/or CQ in the culture medium. γ-Tubulin was used as a loading control. (Scale bars: 50 μm.) (*E*) Fold change in survival relative to untreated controls of WT or Atg7$^{fl/fl}$ organoids in the presence of 4OHT (control [Ctrl], $n = 8$ WT and $n = 9$ Atg7$^{fl/fl}$ mice) and in the presence or absence of MDP, lipopolysaccharide (LPS), flagellin, polyinosinic:polycytidylic acid (PolyIC), or lipoteichoic acid (LTA) in the culture medium ($n = 3$ mice per condition). Significant differences are shown with asterisks. *$P < 0.05$; ***$P < 0.005$.

flux (Fig. 6*D*). These findings suggest that organoid survival is not solely affected by the intrinsic effect of autophagy inhibition on Lgr5^{+}ISC itself but also, by exposure to the gut microenvironment. We, therefore, investigated the direct impact of the microbiota by adding various purified microbial molecules to organoids derived from VillinCreER^{T2}Atg7$^{fl/fl}$ mice and treated ex vivo with 4OHT. We investigated several microbe-associated molecular patterns and found that only muramyl dipeptide (MDP) induced the death of Atg7-deficient organoids but not WT organoids (Fig. 6*E*). Overall, our data suggest a role for Atg7 in the protection and maintenance of Lgr5^{+}ISC in response to not only intrinsic signals, such as DNA damage and ROS, but also, specific microbial signals, such as MDP.

p53 Ablation in Atg7-Deficient Lgr5^{+}ISC Favors Tumor Growth. Given the involvement of Atg7 in the ability of Lgr5^{+}ISC to handle both intrinsic and extrinsic stressors, we reasoned that, in a context of Atg7 deficiency, the induction of apoptosis by p53 might be essential to remove damaged Lgr5^{+}ISC and preserve the integrity of the active stem cell pool.

Notably, as expected, accumulation of abnormal mitochondria still occurs in Atg7$^{-/-}$p53$^{-/-}$ mice, and ROS accumulation was observed in Atg7$^{-/-}$p53$^{-/-}$ organoids (*SI Appendix*, Fig. S7 *A* and *B*). This is consistent with the requirement for autophagy to maintain the pool of functional mitochondria to avoid ROS accumulation. In agreement with the effect of loss of p53 on cell survival, 4OHT treatment of organoids derived from VillinCreER^{T2}Atg7$^{fl/fl}$p53$^{fl/fl}$ mice preserves against the death induced by MDP (*SI Appendix*, Fig. S7 *C* and *D*).

We tested the long-term effects of the simultaneous loss of ATG7 and p53 on intestinal epithelial cells in Atg7$^{-/-}$p53$^{-/-}$ mice over long periods of time. Atg7$^{-/-}$ mice develop no spontaneous intestinal tumors for up to 12 mo after tamoxifen injection. As previously reported (13, 14), we found that p53 knockout in intestinal epithelial cells was not sufficient to initiate intestinal neoplasia during the first 12 mo after tamoxifen injection, with only a few tumors detected at this time point. By contrast, Atg7$^{-/-}$p53$^{-/-}$ mice harbored many adenomas 12 mo after tamoxifen injection (Fig. 7*A*). β-Catenin staining revealed that the tumors in aged Atg7$^{-/-}$p53$^{-/-}$ mice were highly heterogeneous (Fig. 7*B*), with both strongly β-catenin–positive tumors and the punctiform staining of isolated cells within a β-catenin–negative tumor mass. In some cases, these two profiles were observed within the same adenoma. These findings indicate that the tumors of these mice probably arose through diverse pathways and mutational events. Consistent with this hypothesis, γH2AX levels were higher in both the healthy mucosa and adenomas of Atg7$^{-/-}$p53$^{-/-}$ mice (Fig. 7*C*) than in those of p53$^{-/-}$ mice. These results suggest that the combined loss of Atg7 and p53 leads to the accumulation of DNA damage within ISC that is not eliminated and over time, promotes sporadic tumor formation. Atg7 and p53, therefore, act together to preserve the genomic integrity of the Lgr5^{+}ISC pool.

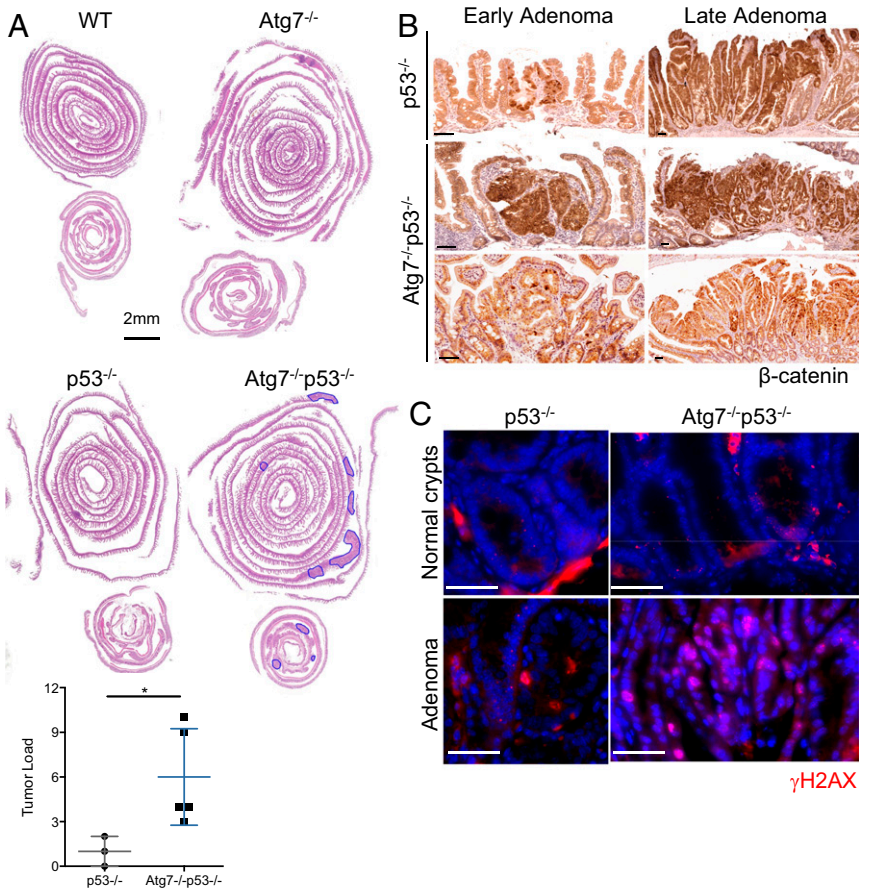

Fig. 7. p53 blocks tumor initiation in the Atg7-deficient intestinal epithelium. (*A*) Representative hematoxylin and eosin staining of tissue sections of small intestinal and colonic "Swiss rolls" from WT, Atg7$^{-/-}$, p53$^{-/-}$, and Atg7$^{-/-}$p53$^{-/-}$ mice killed 12 mo after tamoxifen treatment. Quantification of histologically assessed tumor load in p53$^{-/-}$ or Atg7$^{-/-}$p53$^{-/-}$ mice 12 mo after tamoxifen treatment ($n = 3$ p53$^{-/-}$ and $n = 5$ Atg7$^{-/-}$p53$^{-/-}$ mice). Tumors are circled in blue. (Scale bar: 2 mm. Significant differences are shown with asterisks. *$P < 0.05$.) (*B*) Representative β-catenin staining on small polyps (*Left*) and adenomas (*Right*) from p53$^{-/-}$ and Atg7$^{-/-}$p53$^{-/-}$ mice killed 12 mo after tamoxifen treatment. (Scale bars: 50 μm.) (*C*) Representative γH2AX staining on healthy crypts and adenomas from p53$^{-/-}$ and Atg7$^{-/-}$p53$^{-/-}$ mice killed 12 mo after tamoxifen treatment. (Scale bars: 50 μm.)

Discussion

We show here that Atg7 is critical for the integrity of Lgr5^{+}ISC through both cell-autonomous and noncell-autonomous effects. We found that Atg7 in Lgr5^{+}ISC affects the cytoplasmic removal of dysfunctional mitochondria threatening genomic integrity from the cytoplasm and alters the ROS antioxidant response. Our results exhibit similarities with previous work, which reports that Atg5 is important for the maintenance of Lgr5^{+}ISC by reducing excessive ROS (7). Mice lacking ATG5 in intestinal epithelial cells had significantly fewer Lgr5^{+}ISC than control mice and showed impaired ISC-dependent intestinal regeneration after irradiation. Accordingly to our results, treating Atg5-deficient mice with an antioxidant rescued theses defects. Our study expands these findings and demonstrates that Atg7 promotes ISC fitness by activating DNA repair. We also showed that p53 functions as a gatekeeper to eliminate unrepaired damaged in Atg7-deficient Lgr5^{+}ISC. Concomitant deletion of Atg7 and p53 allows the persistence of damaged Lgr5^{+}ISC and increases the occurrence of dysplastic lesions in the gut. In addition, we demonstrated that Atg7 also has noncell-autonomous functions in Lgr5^{+}ISCs in which it alters the dialogue between these cells and the microbiota, disrupting their integrity. Importantly, Atg7-deficient mice exhibit certain similarities with Atg5-deficient mice, which validates a role for autophagy in ISC maintenance and regeneration. However, some discrepancies between these two studies persist. Whereas Atg5 deletion reduces the number of Lgr5^{+}ISCs, we did not observe any decreased in ISC number in mice lacking Atg7 since the death of ISC is associated with an amplification of the Lgr5^{+}ISC pool, indicating that the reserve pool of ISC and/or committed progenitors are able to maintain ISC homeostasis. In addition, in contrast to our study, Atg5 deletion affects Lgr5^{+}ISC survival through a cell-autonomous mechanism with no microbiota-related effect. Importantly, accumulating evidences suggest additional and nonoverlapping functions for Atg protein including cell survival and apoptosis, modulation of cell traffic, protein secretion, transcription, translation, and membrane reorganization (15, 16). In particular, independently of its function in autophagy, Atg7 modulates p53 activity to regulate cell cycle and survival during metabolic stress. It has been shown that, on metabolic stresses, the absence of Atg7 in mouse embryonic fibroblast increases DNA damage and p53-dependent apoptosis. Future studies need to be performed to clarify the mechanism involved in the loss of Lgr5^{+}ISC in Atg5-deficient mice and to test the involvement of p53. Conflicting results between the loss of Atg5 and Atg7 in Lgr5^{+}ISC could be caused by the potential loss of nonautophagic functions associated with individual ATG proteins.

The persistence of stem cells in tissues for extended periods of time increases the risk of mutations accumulating. It has been suggested that stem cells may have a greater capacity than other cells to repair DNA or to resist elimination when damaged (17).

However, much remains unknown about the mechanisms by which DNA damage is repaired in adult stem cells. The two principal and complementary mechanisms by which eukaryotic cells repair double-strand breaks are homologous recombination (HR) and nonhomologous end joining (NHEJ). NHEJ-type repair is more error prone than HR-type repair and often leads to misrepaired double-strand breaks that may result in chromosomal deletions, insertions, or translocations and genomic instability. Our data indicate that autophagy plays a crucial role in maintaining the genomic integrity of Lgr5$^+$ISC by regulating DNA repair pathways. Evidence from ex vivo studies suggests that autophagy can control DNA damage repair directly by increasing the proteasomal degradation of HR repair-mediating proteins, such as CHK1, RAD51, and FLNA, or by increasing levels of p62, which has recently emerged as an important mediator of HR repair (18–20). Our genome-wide transcriptome profiling of Lgr5$^+$ISC suggests that a lack of Atg7 alters the DNA repair gene signature and is predictive of defective HR repair. Consistent with this notion, our data indicate that the lack of Atg7 specially affected the integrity of Lgr5$^+$ISC, leading to a lower efficiency of double-strand break repair, and that p53 signaling functions as a gatekeeper for the initial damage response. In this scenario, the error-prone process of NHEJ repair could protect Lgr5$^+$ISC, ensuring intestinal homeostasis. However, our data indicate that, in the long term, the loss of p53 promotes DNA damage and tumor formation in Atg7-deficient Lgr5$^+$ISC. This protumorigenic effect of autophagy inhibition is at odds with the antitumoral function of Atg7 previously reported in our previous study of a mouse model of Apc-induced colon cancer (6). In this previous study, we found that Atg7 deletion in the intestinal epithelium of APC$^{+/-}$ mice resulted in an antitumoral immune response mediated by changes in gut microbiota composition. We also reported an enhancement of p53 activity linked to the deletion of Atg7. The results presented here highlight the key function of p53 in counteracting the adverse effect of Atg7 inhibition by eliminating damage and potential tumor-initiating ISC and suggest that the enhancement of p53 activation induced by a lack of Atg7 may also contribute to tumor suppression.

We used a functional approach to investigate the role of Atg7 in the mechanisms of DNA repair in response to genotoxic challenges, such as irradiation, oxaliplatin, and doxorubicin treatments. We found that Atg7 protected against these genotoxic stresses specifically in Lgr5$^+$ISC but not in other intestinal epithelial cells. Loss of Atg7 increased double-strand break formation and apoptosis in Lgr5$^+$ISC, whereas the activation of autophagy induced by 24 h of fasting increased the DNA repair capacity of Lgr5$^+$ISC and decreased the apoptosis of these cells. By contrast, fasting did not protect progenitors from the effects of genotoxic treatments. Interestingly, fasting has been proposed as a means of reducing host toxicity in patients undergoing high-dose chemotherapy through the preservation of ISC viability (21). Our data support this approach and suggest that autophagy is a crucial effector of fasting effects. Our data indicate that Lgr5$^+$ISC are uniquely equipped to preserve their genome integrity and that autophagy provides these cells with DNA damage repair pathways for their protection. Given that fasting may be challenging to employ in cancer patients, it will be important to evaluate the effect of rapamycin, a potent activator of autophagy, on the gut toxicity mediated by genotoxic stresses (irradiation, chemotherapeutic treatments). The clinical application of these findings for colon cancer treatment should be further investigated.

It has been proposed, consistent with our findings, that Lgr5$^+$ISC may be more radioresistant to DNA damage than the other crypt cells (3, 22), including progenitors and the pool of quiescent ISC, which are located farther away from the crypt base and express Bmi1 and Hopx. However, the radio resistance of Lgr5$^+$ISC and their quiescent counterparts remain a matter of debate. Several lines of evidence suggest that mitotically active Lgr5$^+$ISC are more sensitive than other cells to irradiation (23, 24). One possible explanation reconciling this paradox is that quiescent and mitotically active Lgr5$^+$ISC have a number of expression markers, including Lgr5, in common (25). Subpopulations of Lgr5$^+$ISC with different DNA repair pathways may then participate in the different sensitivities of the Lgr5$^+$ subpopulation. Further examinations of single-cell analyses of the Lgr5 subpopulation are required to define the DNA repair and response pathways.

At the noncell-autonomous level, we showed that the death of Atg7-deficient Lgr5$^+$ISC was dependent on the microbiota. The inhibition of autophagy in the intestinal organoids either by the conditional deletion of Atg7 upon the presence of 4OHT or by the addition of chloroquine to the medium had no effect on organoid survival. By contrast, in vivo, the treatment of Atg7$^{-/-}$ mice with broad-spectrum antibiotics decreased DNA damage and increased the survival of Atg7-deficient Lgr5$^+$ISC. Surprisingly, we found that the deletion of Atg7 affected organoid survival only if *Atg7* was knocked out in vivo before culture. This suggests that microenvironmental signals in Atg7-deficient mice induce lasting deleterious effects in Lgr5$^+$ISC contributing to their death. Both our data and previous studies have shown that Atg7$^{-/-}$ mice present a defect of antimicrobial peptide production and secretion, which is thought to be involved in direct cross-talk between bacteria and Lgr5$^+$ISC (6, 26). The microbiota may, therefore, also contribute to the accumulation of intrinsic stress in Atg7-deficient Lgr5$^+$ISC. We tested the effects of several bacterial products on Atg7-deficient organoids, but only MDP affected the survival of these organoids. MDP has been shown to exert cytoprotective effects on Lgr5$^+$ISC through its intracellular receptor NOD2 (27), which is known to interact directly with the autophagy machinery (28–30). Autophagy may, therefore, mediate the cytoprotective response to MDP and could, more generally, act as an essential protective layer in the Lgr5$^+$ISC response to specific microbial signals.

Finally, our results indicate that the loss of Atg7 promotes excessive generation and abnormal clearance of ROS in Lgr5$^+$ISC, leading to the apoptosis of these cells. We show that, following the loss of *Atg7*, Lgr5$^+$ISC accumulate both mitochondrial superoxide and cytoplasmic ROS due to a defective antioxidant response. DNA damage and poor survival in autophagy-deficient Lgr5$^+$ISC can be reduced by treatment with NAC or antibiotics. These results suggest that the microbiota acts as an exogenous source of ROS and that excessive ROS production is responsible for the elimination of Lgr5$^+$ISC. Intriguingly, the loss of Atg7 led to loss of the master regulator of the antioxidant response specifically in the Lgr5$^+$ISC but not in other intestinal epithelial cells, which displayed an antioxidant response. It is intriguing that the NRF2 response in Lgr5$^+$ISC is the opposite of that in progenitors and differentiated cells, and this finding highlights the specificity and importance of dynamic redox control in stem cell function. The mechanism of NRF2 repression in Lgr5$^+$ISC is currently unclear, but similar observations have been reported for *Drosophila*. In conditions of oxidative stress, NRF2 activity is repressed in ISC, contrasting with the situation in differentiated cells (31).

In conclusion, we suggest that Atg7 acts as a gatekeeper of Lgr5$^+$ISC integrity, which is required for the maintenance of robust antioxidant defenses and DNA repair to minimize the effects of intrinsic and environmental stresses. This work may also have direct clinical applications in the minimalization of adverse effects of chemotherapy on ISC survival or the sensitization of cancer cells to chemotherapy.

Methods

Mouse Models and Treatments. Mice carrying floxed alleles of the *Atg7* gene (11), mice carrying floxed alleles of the *P53* gene (32), or both were crossed with VillinCreER^{T2} mice (33) or Lgr5-EGFP-IRES-CreER^{T2} mice (23). All experiments were carried out in the C57BL/6 background and housed in conventional conditions. All animal experiments were carried out under approval by the Animal Care and Use Commitee of Institut Cochin and by the French Ministry of Agriculture (2018-20094). Tamoxifen injections were performed on 2- to 3-mo-old mice. Both male and female mice were used. Mice received intraperitoneal injections of 1 mg tamoxifen, and their diet was supplemented with tamoxifen for 5 d/mo. Unless otherwise indicated, mice were killed 1 mo after tamoxifen treatment. For proliferation studies, BrdU (2.5 mg; Sigma-Aldrich) was injected into the mice 1.5 h before they were killed. For irradiation studies, mice were exposed to a ^{137}Cs source of γ-irradiation at a dose rate of 1.47 Gy/min, with a final dose of 10 Gy, and they were then killed 6 h later. For chemotherapy treatments, mice were either fasted or fed ad libitum for 24 h and then treated with 10 mg/kg oxaliplatin or 20 mg/kg doxorubicin (Sigma-Aldrich) intraperitoneally for 6 h before death. For NAC treatment, 12.5 mg/mL NAC was added to the drinking water (for an estimated intake of 200 mg/kg per day), and the pH was adjusted as appropriate. The water was changed every other day for a month following tamoxifen treatment. For antibiotic treatment, we added a combination of 1 g/L ampicillin, 1 g/L neomycin, 1 g/L metronidazole, and 0.5 g/L vancomycin (Sigma-Aldrich) to the drinking water of the mice. This solution was replaced every other day for a month following tamoxifen treatment.

Data Availability. All relevant data, associated protocols, and materials are present in *SI Appendix*.

ACKNOWLEDGMENTS. We thank M. Komatsu (Niigata University), S. Robine (Institut Curie), A. Berns (Netherlands Cancer Institute), and H. Clevers (Hubrecht Institute) for supplying mutant mice. We also thank the staff of the Cochin animal facility. This work was supported by the Fondation ARC (Association pour la Recherche sur le Cancer), the Institut National du Cancer, the Comité de Paris de la Ligue Contre le Cancer, the Agence National de la Recherche, and the National Institute of Health and Medical Research (France). C.T. was supported by a fellowship from the Ministère de la Recherche et de l'Enseignement Supérieur, la Fondation ARC, and the Labex Who Am I?.

1. A. Durand *et al*., Functional intestinal stem cells after Paneth cell ablation induced by the loss of transcription factor Math1 (Atoh1). *Proc. Natl. Acad. Sci. U.S.A.* **109**, 8965–8970 (2012).
2. N. Barker, Adult intestinal stem cells: Critical drivers of epithelial homeostasis and regeneration. *Nat. Rev. Mol. Cell Biol.* **15**, 19–33 (2014).
3. C. Metcalfe, N. M. Kljavin, R. Ybarra, F. J. de Sauvage, Lgr5+ stem cells are indispensable for radiation-induced intestinal regeneration. *Cell Stem Cell* **14**, 149–159 (2014).
4. N. Barker *et al*., Crypt stem cells as the cells-of-origin of intestinal cancer. *Nature* **457**, 608–611 (2009).
5. N. Mizushima, A brief history of autophagy from cell biology to physiology and disease. *Nat. Cell Biol.* **20**, 521–527 (2018).
6. J. Lévy *et al*., Intestinal inhibition of Atg7 prevents tumour initiation through a microbiome-influenced immune response and suppresses tumour growth. *Nat. Cell Biol.* **17**, 1062–1073 (2015).
7. J. Asano *et al*., Intrinsic autophagy is required for the maintenance of intestinal stem cells and for irradiation-induced intestinal regeneration. *Cell Rep.* **20**, 1050–1060 (2017).
8. S. Bel *et al*., Paneth cells secrete lysozyme via secretory autophagy during bacterial infection of the intestine. *Science* **357**, 1047–1052 (2017).
9. K. Cadwell *et al*., A key role for autophagy and the autophagy gene Atg16l1 in mouse and human intestinal Paneth cells. *Nature* **456**, 259–263 (2008).
10. L. C. Gomes, G. Di Benedetto, L. Scorrano, During autophagy mitochondria elongate, are spared from degradation and sustain cell viability. *Nat. Cell Biol.* **13**, 589–598 (2011).
11. M. Komatsu *et al*., Impairment of starvation-induced and constitutive autophagy in Atg7-deficient mice. *J. Cell Biol.* **169**, 425–434 (2005).
12. M. Komatsu *et al*., The selective autophagy substrate p62 activates the stress responsive transcription factor Nrf2 through inactivation of Keap1. *Nat. Cell Biol.* **12**, 213–223 (2010).
13. M. Chanrion *et al*., Concomitant Notch activation and p53 deletion trigger epithelial-to-mesenchymal transition and metastasis in mouse gut. *Nat. Commun.* **5**, 5005 (2014).
14. S. Schwitalla *et al*., Loss of p53 in enterocytes generates an inflammatory microenvironment enabling invasion and lymph node metastasis of carcinogen-induced colorectal tumors. *Cancer Cell* **23**, 93–106 (2013).
15. S. Subramani, V. Malhotra, Non-autophagic roles of autophagy-related proteins. *EMBO Rep.* **14**, 143–151 (2013).
16. B. Levine, G. Kroemer, Biological functions of autophagy genes: A disease perspective. *Cell* **176**, 11–42 (2019).
17. I. Vitale, G. Manic, R. De Maria, G. Kroemer, L. Galluzzi, DNA damage in stem cells. *Mol. Cell* **66**, 306–319 (2017).
18. G. Hewitt *et al*., SQSTM1/p62 mediates crosstalk between autophagy and the UPS in DNA repair. *Autophagy* **12**, 1917–1930 (2016).
19. E. Y. Liu *et al*., Loss of autophagy causes a synthetic lethal deficiency in DNA repair. *Proc. Natl. Acad. Sci. U.S.A.* **112**, 773–778 (2015).
20. Y. Wang, W. G. Zhu, Y. Zhao, Autophagy substrate SQSTM1/p62 regulates chromatin ubiquitination during the DNA damage response. *Autophagy* **13**, 212–213 (2017).
21. K. L. Tinkum *et al*., Fasting protects mice from lethal DNA damage by promoting small intestinal epithelial stem cell survival. *Proc. Natl. Acad. Sci. U.S.A.* **112**, E7148–E7154 (2015).
22. G. Hua *et al*., Crypt base columnar stem cells in small intestines of mice are radioresistant. *Gastroenterology* **143**, 1266–1276 (2012).
23. N. Barker *et al*., Identification of stem cells in small intestine and colon by marker gene Lgr5. *Nature* **449**, 1003–1007 (2007).
24. K. S. Yan *et al*., The intestinal stem cell markers Bmi1 and Lgr5 identify two functionally distinct populations. *Proc. Natl. Acad. Sci. U.S.A.* **109**, 466–471 (2012).
25. S. Itzkovitz *et al*., Single-molecule transcript counting of stem-cell markers in the mouse intestine. *Nat. Cell Biol.* **14**, 106–114 (2011).
26. K. Cadwell, K. K. Patel, M. Komatsu, H. W. Virgin 4th, T. S. Stappenbeck, A common role for Atg16L1, Atg5 and Atg7 in small intestinal Paneth cells and Crohn disease. *Autophagy* **5**, 250–252 (2009).
27. G. Nigro, R. Rossi, P. H. Commere, P. Jay, P. J. Sansonetti, The cytosolic bacterial peptidoglycan sensor Nod2 affords stem cell protection and links microbes to gut epithelial regeneration. *Cell Host Microbe* **15**, 792–798 (2014).
28. S. Chauhan, M. A. Mandell, V. Deretic, IRGM governs the core autophagy machinery to conduct antimicrobial defense. *Mol. Cell* **58**, 507–521 (2015).
29. R. Cooney *et al*., NOD2 stimulation induces autophagy in dendritic cells influencing bacterial handling and antigen presentation. *Nat. Med.* **16**, 90–97 (2010).
30. L. H. Travassos *et al*., Nod1 and Nod2 direct autophagy by recruiting ATG16L1 to the plasma membrane at the site of bacterial entry. *Nat. Immunol.* **11**, 55–62 (2010).
31. C. E. Hochmuth, B. Biteau, D. Bohmann, H. Jasper, Redox regulation by Keap1 and Nrf2 controls intestinal stem cell proliferation in Drosophila. *Cell Stem Cell* **8**, 188–199 (2011).
32. J. Jonkers *et al*., Synergistic tumor suppressor activity of BRCA2 and p53 in a conditional mouse model for breast cancer. *Nat. Genet.* **29**, 418–425 (2001).
33. F. el Marjou *et al*., Tissue-specific and inducible Cre-mediated recombination in the gut epithelium. *Genesis* **39**, 186–193 (2004).